8.07f/W(Jul162004) +model | RENE : 2741 | Prod.Type:FTP pp.1–10(col.fig.:2,5–10,12–17) | ED:PraveenNC PAGN:Bala SCAN:

ARTICLE IN PRESS

Available online at www.sciencedirect.com

ScienceDirect

ELSEVIER

Renewable Energy ▮ (▮▮▮▮) ▮▮▮–▮▮▮

RENEWABLE ENERGY

www.elsevier.com/locate/renene

Application of fluid–structure interaction simulation of an ocean wave energy extraction device

Emmanuel B. Agamloh[1], Alan K. Wallace[2], Annette von Jouanne*

School of Electrical Engineering and Computer Science, Oregon State University, Corvallis, OR 97331, USA

Abstract

A numerical technique that employs a computational fluid dynamics (CFD) code is used to perform coupled fluid–structure interaction simulation of a wave energy device in order to assess power output in a 3D numerical wave flume. The current method determines the motion of the buoy from the dynamic solution of the fluid flow problem and the dynamic buoy motion problem rather than prescribing the motion of the buoy. The power output of the device is calculated for different wave conditions. The technique was expanded for an array of two buoys to determine the interference between them.
© 2007 Elsevier Ltd. All rights reserved.

Keywords: Ocean wave energy; Computational fluid dynamics; Buoy

1. Introduction

The analysis of ocean wave energy conversion devices (OWECs) has been largely based on linear potential flow theory in which time domain or frequency domain solutions are obtained usually with assumptions of small amplitude oscillations (linearity). However, practical OWECs require large amplitude oscillations and non-linear effects become an issue. Also, these devices are usually "tuned" to take advantage of resonance. The time domain solutions required have been enhanced with the availability of commercial computational fluid dynamics (CFD) software, to iteratively solve the Navier–Stokes equations. The iterative nature of these fluid solvers also makes it convenient to include the effects of the generators or power take-off (PTOs) mechanisms of the wave energy device, which is generally a non-linear phenomenon.

In this paper, a commercial CFD code has been used to simulate a heaving buoy OWEC. The buoy is excited by regular waves that are generated in a 3D numerical wave tank (NWT) and is free to move in response to the waves. The present work is limited to single degree of freedom (SDOF) heave but can be expanded to include all six degrees of freedom. The fluid–structure interaction (FSI) model also includes modeling the free surface using the volume of fluid (VOF) technique, with the high resolution interface capturing (HRIC) method, which accurately predicts the arbitrary deformation of the air–water interface. The PTO is represented as a damping system across which the energy is captured.

2. Numerical method

2.1. Governing equations

Generally, in a coupled FSI simulation, a fluid dynamics problem is discretized and solved using the fluid flow solver to obtain the forces on the structure. Then the structure motion dynamics is solved using the forces obtained from the fluid solver and other external forces that are pertinent to the problem being solved. The basic mathematical model for the discretization process is the fundamental governing equations of fluid motion, known as the Navier–Stokes (NS) equations. These are a set of equations derived from the conservation laws (mass, energy, momentum, and

*Corresponding author. Tel.: +1 541 737 0831; fax: +1 541 737 1300.
E-mail addresses: eagamloh@advancedenergy.org (E.B. Agamloh), wallace@eecs.oregonstate.edu (A.K. Wallace), avj@eecs.oregonstate.edu (A. von Jouanne).
[1]Currently with Advanced Energy Corporation, Raleigh, NC 27606, USA.
[2]Deceased.

0960-1481/$ - see front matter © 2007 Elsevier Ltd. All rights reserved.
doi:10.1016/j.renene.2007.04.010

UNCORRECTED PROOF

Please cite this article as: Agamloh EB, et al. Application of fluid–structure interaction simulation of an ocean wave energy extraction device. Renew Energy (2007), doi:10.1016/j.renene.2007.04.010

Nomenclature

m	mass
F_{wave}	wave force
F_{PTO}	power take-off force
$U, \dot{U}, \ddot{U}$	buoy displacement, velocity, acceleration (x, y, z)
λ	wavelength
k	wave number
d	diameter of buoy
x, y, z	Cartesian coordinate system
s	stroke
a	amplitude of wave maker plunger motion
p	pressure
τ	viscous shear stress
c	volume fraction
v	continuum velocity
v_s	surface velocity of cell volume
μ_{eff}	effective dynamic viscosity of fluid
S	cell face area
V	cell volume
H_s	significant wave height
T	wave period
h	water depth
η	water surface elevation
P_{cap}	power captured

angular momentum, all of which are conserved in a closed volume). These equations together with the continuity equation constitute the fundamental set of equations that are discretized and solved by the flow solver.

In most engineering problems, there are fluctuations of all the fluid flow quantities in space and time due to turbulence, however, their average values can be considered to be steady. The NS equations that include the effects of turbulence by using the mean fluid flow quantities are known as Reynolds averaged Navier–Stokes equations (RANSE). In the RANSE the flow quantities are formulated in "Reynold's averaged quantities", by which each dependent variable is expressed as a sum of its time-averaged mean value and a fluctuating component [7] (Fig. 1).

In integral form the fundamental equations are given by

$$\frac{\mathrm{d}}{\mathrm{d}t}\int_V \rho u_i \,\mathrm{d}V + \int_S \rho u_i (v - v_s)\,\mathrm{d}s = \int_S (\tau_{ij} - p)\,\mathrm{d}s + \int_V \rho g \,\mathrm{d}V, \tag{1}$$

$$\frac{\mathrm{d}}{\mathrm{d}t}\int_V \rho \,\mathrm{d}V + \int_S \rho (v - v_s)\,\mathrm{d}s = 0, \tag{2}$$

where v_s is the surface velocity of cell volume, v is continuum velocity, V the volume bounded by a closed surface S, g the acceleration due to gravity, $\tau_{ij} = \mu_{eff}(\partial u_i/\partial x_j + \partial u_j/\partial x_i)$ are the effective stresses and μ_{eff} the effective dynamic viscosity of the fluid.

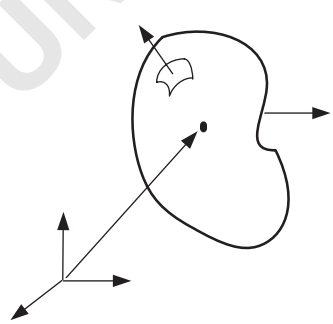

Fig. 1. Control volume.

The fluid solver, Comet, is an unstructured finite volume code developed by the CD-Adapco group. This software has been previously described and validated in publications such as [1–3]. Comet is a general purpose CFD code with an efficient set of numerical solution algorithms that can be used to solve both fluid and solid mechanics problems. One feature of the solver that was employed in this work is the ability of the user to generate the grid in blocks with any given blocks not necessarily matching at their interface. Also, there are features that enable two blocks of the grid to slide against each other, thus a part of the grid that contains the buoy can be moved or regenerated while the far field grids may remain stationary. The moving of the grid in the fixed global coordinate systems where the RANSE equations are expressed requires the space conservation law, which ensures that the volume of the cells is conserved, even though their shapes change as a result of moving the grid. This law is expressed as

$$\frac{\mathrm{d}}{\mathrm{d}t}\int_V \mathrm{d}V - \int_S v_s \,\mathrm{d}s = 0. \tag{3}$$

2.2. The numerical grid

The numerical 3D solution grid is shown in Fig. 2. The overall size of the domain is 12 m × 3 m × 3 m and the cylindrical buoy has a diameter of 0.6 m and an equilibrium draft of 0.5 m. The mesh is made up of three main blocks; the middle block is a finer mesh that moves with the buoy. This block is regenerated at every time step to maintain its structural integrity as the buoy moves up and down. This buoy-fitted block is flanked on each side by relatively coarse "stationary" meshes that form part of the solution domain but do not form part of the mesh regeneration procedure at each time step. Furthermore, the "stationary" mesh has variable size with larger sizes towards the wall boundaries to provide damping effect of the waves. The numerical grid is generated using the command language of Comet.

UNCORRECTED PROOF

Please cite this article as: Agamloh EB, et al. Application of fluid–structure interaction simulation of an ocean wave energy extraction device. Renew Energy (2007), doi:10.1016/j.renene.2007.04.010

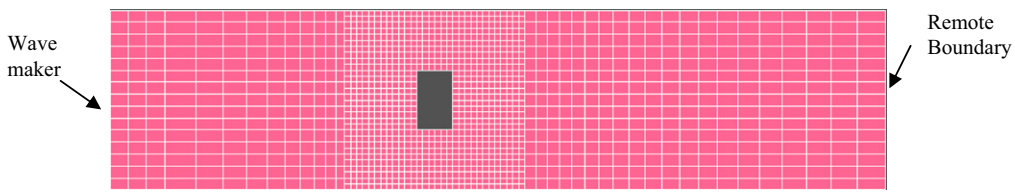

Fig. 2. Numerical grid.

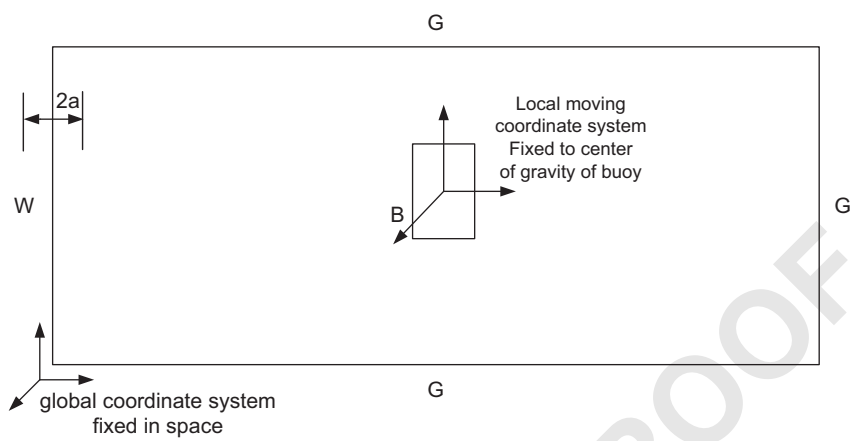

Fig. 3. 2D Representation of the boundaries of the solution domain.

2.3. Boundary conditions

The solution domain is bounded by a wave maker on the left wall boundary. At the wave maker boundary, the horizontal velocity of motion of the boundary is imposed on the water particle velocities at the boundary.

The other boundaries of the solution domain are solid walls where no-slip boundary conditions are applied. The no-slip condition ensures that the fluid moving over a solid surface does not have velocity relative to the surface at the point of contact. For the floating buoy, the no slip condition also means that the vertical heave velocity is imposed on the water particles at the boundary of the buoy (Fig. 3).

2.4. Generation of waves

The waves were generated by a piston type wave maker located at the left boundary of the solution domain. The plunger moves sinusoidally with the functions $= a \sin \omega t$. For most wave tanks, the opposite end of the wave maker is a typical beach which absorbs the waves that are generated, in order to prevent their reflection back into the solution domain. This means either non-reflecting boundaries have to be used or a damping/dissipation zone is added to the solution domain for damping the waves. The non-reflecting boundary option was not feasible in the current work and it was thought that adding a damping zone would increase computational demands. Therefore, in this simulation, the far field boundary is located far enough and simulation time is chosen in such a way to avoid such reflections. Also, the cell volumes located towards the boundaries are made larger and this provided some damping of the waves at the boundaries, adequate enough to avoid wave reflections.

A linear propagating wave generated by a piston wave maker has velocity potential, ϕ, and surface elevation, η, given by [4,5]

$$\phi = \frac{4s \tanh kh \sinh kh}{\omega(2kh + \sin 2kh)} \cosh k(z+h) \cos(kx - \omega t), \tag{4}$$

$$\eta(x,t) = -\left.\frac{\partial \phi}{\partial t}\right|_{z=0} = \frac{4s \sinh^2 kh}{2kh + \sinh 2kh} \sin(kx - \omega t), \tag{5}$$

where s is stroke of the wave maker h is water depth, ω is angular frequency and k is wave number of the generated wave. The expression in Eq. (5) was used as an analytical check on the surface elevation of the waves generated by the wave maker without any buoy in the wave tank.

2.5. Coupling procedure

In previous investigations the motion of the body was prescribed rather than determined [3,6]. In this paper, the motion of the wave energy buoy is obtained from the dynamic system solution of the fluid flow interacting with the buoy structure with due consideration of the damping of the PTO. The model employs a technique in which the mesh moves as the buoy heaves. The instantaneous position of the buoy is determined from the set of add-on codes, implemented in FORTRAN. These additional codes interact with the solver to determine the displacements in

UNCORRECTED PROOF

Please cite this article as: Agamloh EB, et al. Application of fluid–structure interaction simulation of an ocean wave energy extraction device. Renew Energy (2007), doi:10.1016/j.renene.2007.04.010

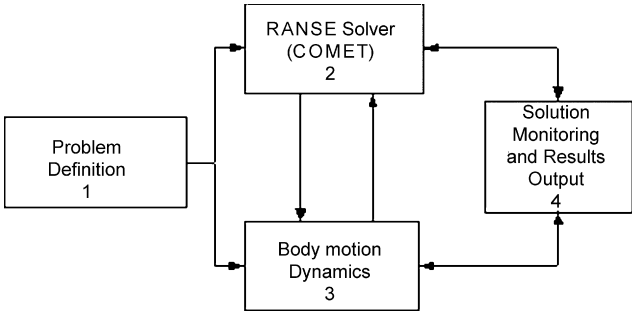

Fig. 4. Block schematic of coupling algorithm.

order to move the buoy to its new position and also to update the boundary conditions. In order to maintain the structural integrity of the fluid mesh, it is regenerated at every time step. For this reason, the solution domain mesh has been generated in a way to enhance mesh regeneration. The grid consists of a fine mesh fitted to the body (regenerated at every time step) and flanked on each side by a relatively coarse mesh that is not regenerated. These blocks are connected together using the explicit connectivity function of the Comet code [7].

The general block schematic of the coupling algorithm is shown in Fig. 4. The motion of the buoy is governed by Newton's second law of motion:

$$m\ddot{U} = F_{wave} + F_g + F_{ext}, \tag{6}$$

where F_{wave} is the wave forces on the buoy, F_g the weight of the buoy, F_{ext} the external force on the buoy, m the mass of the buoy, $\ddot{U}$ the acceleration of buoy. Following Azcueta [8], the wave force on the buoy can be calculated as the integration of the pressure field and viscous stresses on the instantaneous wetted surface of the buoy by the following expression:

$$F_{wave} = \sum_{j=1}^{n}(-p_j n_j + \tau_j)S_j, \tag{7}$$

where p is the pressure, n is the normal vector to each cell face, τ is the tangential viscous shear stress on the cell face and S is the cell face area. The force F_g is the weight of the buoy which acts in the negative z-direction and the force F_{ext} is any external force that comes into play for the particular degree of freedom. In this problem, examples of this force are PTO force, or restraint forces as provided by tethers and moorings. For this device, the PTO is represented as a damper. Therefore, the PTO force on the buoy and the pneumatic power across the damper are respectively given by Eq. (8). Note here that the pneumatic power is calculated as the product of the vertical heave velocity and the damping force.

$$F_{pto} = b_1\dot{U}, \quad P_{pto} = b_1 \cdot \dot{U} \cdot \dot{U}, \tag{8}$$

where b_1 is the power absorbing damping coefficient and $\dot{U}$ the velocity, in this particular case vertical heave velocity.

Eq. (6) is essentially, a set of three translational equations in each of the three coordinate directions x, y, z. For non-spherical buoys such as the buoy under consideration in this study, any possible rotation is important because it could affect the translational motions. Therefore, in addition to the translational equations, the angular momentum has to be solved to yield additional equations. Since the buoy was constrained to heave only, all rotational motions were curtailed and this step was unnecessary. For Eq. (6), expressed in the form, $m\ddot{U} = F$, the left side of the equation can be integrated from t_{n-1} to t_n exactly. The right-hand side requires approximation of some mean value of F (which incorporates the convective and diffusive fluxes and source terms) over the interval of integration. Consequently, the velocity and displacements in Eq. (6) can be written as follows:

$$\dot{U}_{n+1} = \dot{U}_n + \frac{\Delta t}{m}\hat{F}, \tag{9}$$

$$U_{n+1} = U_n + \Delta t \cdot \hat{\dot{U}}, \tag{10}$$

where $\hat{F}$ is the mean value of the resultant force and $\hat{\dot{U}}$ the mean value of the velocity, U_{n+1} and $\dot{U}_{n+1}$ are displacement and velocity of the current time step, U_n and $\dot{U}_n$ are displacement and velocity of the previous time step and Δt is a carefully chosen time step. There are numerous methods by which $\hat{F}$ and $\hat{\dot{U}}$ can be approximated. Azcuetta [8] approximated the average values of velocity and force with the following expressions:

$$\hat{F} = \tfrac{1}{2}(F_n + F_{n-1}), \tag{11}$$

$$\hat{\dot{U}} = \tfrac{1}{2}(U_{n+1} + U_n). \tag{12}$$

This integration scheme employs the trapezoidal rule for obtaining the velocity and Crank–Nicholson integration method for obtaining the displacement. The widely used Newmark time integration scheme approximates the velocity and displacement as follows:

$$\dot{U}_{n+1} = \dot{U}_n + \Delta t_n((\tfrac{1}{2} - \gamma)\ddot{U}_n + \gamma\ddot{U}_{n+1}) \tag{13}$$

$$U_{n+1} = U_n + \Delta t_n\dot{U}_n + \Delta t_n^2((\tfrac{1}{2} - \beta)\ddot{U}_n + \beta\ddot{U}_{n+1}), \tag{14}$$

where γ and β are constants. The hybrid Crank–Nicholson method proposed in [8] was compared to the unconditionally stable Newmark method, with parameters $\beta = 0.5$, $\gamma = 0.25$ and both time integration methods were found to be stable and gave similar results as shown in Fig. 5 ($T = 2.5$ s).

2.6. Free surface

The air and water in the solution domain are replaced by an "effective fluid" whose properties depend on the physical properties of the constituent fluids and a scalar indicator function, known as the volume fraction, c. The volume fraction is assigned a value of one (1) for cells filled with water and a value of zero (0) for cells filled with air.

UNCORRECTED PROOF

Please cite this article as: Agamloh EB, et al. Application of fluid–structure interaction simulation of an ocean wave energy extraction device. Renew Energy (2007), doi:10.1016/j.renene.2007.04.010

The transport equation (15) is solved for the volume fraction using computed current values of the velocity field:

$$\frac{\mathrm{d}}{\mathrm{d}t}\int_V c\cdot \mathrm{d}V + \int_S c\cdot(v - v_s)\,\mathrm{d}S = 0, \tag{15}$$

where v is the velocity of the particle, v_s is the characteristic velocity of the fluid, V is the cell volume and S is the area of the cell face. The HRIC technique is used for capturing the deformation of the free surface [9]. The HRIC method is based on a convective transport of the scalar quantity c which indicates the presence of either air or water. The scheme is a non-linear blend of upwind and downwind differencing schemes designed to provide a sharp interface between the two fluids. In Fig. 6, the cylindrical buoy is shown in the NWT with a capture of the free water surface at four time instants.

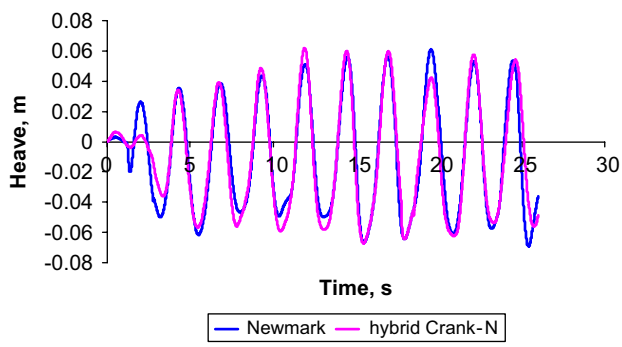

Fig. 5. Heave displacement with different numerical time integration schemes.

The velocity vectors shown in Fig. 7 depict the flow around the buoy. As the buoy moves up, naturally the water particles will tend to move into the void created by the buoy, hence we see the velocity vectors pointing up as shown in the figure. The opposite effect takes place when water particles are moved ahead of the buoy as it moves down. Thus the velocity vectors point downwards and are displaced from the buoy. This velocity vector distribution is similar to patterns reported in [6] under prescribed oscillation.

2.7. Power absorption coefficient

In this simulation the power absorption coefficient in Eq. (8), b_1 has been assumed to be a constant value throughout

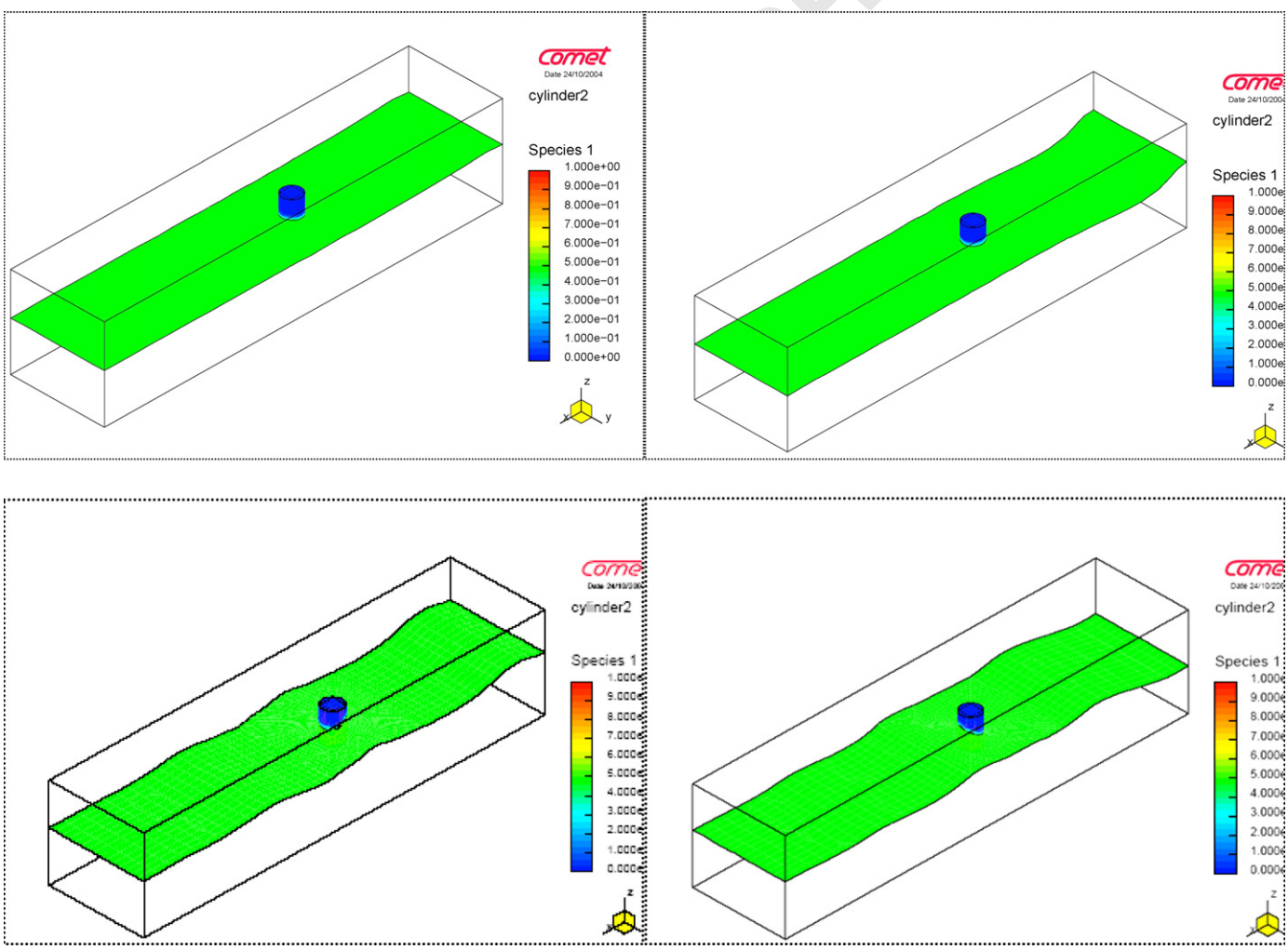

Fig. 6. Free surface capturing (single buoy).

Please cite this article as: Agamloh EB, et al. Application of fluid–structure interaction simulation of an ocean wave energy extraction device. Renew Energy (2007), doi:10.1016/j.renene.2007.04.010

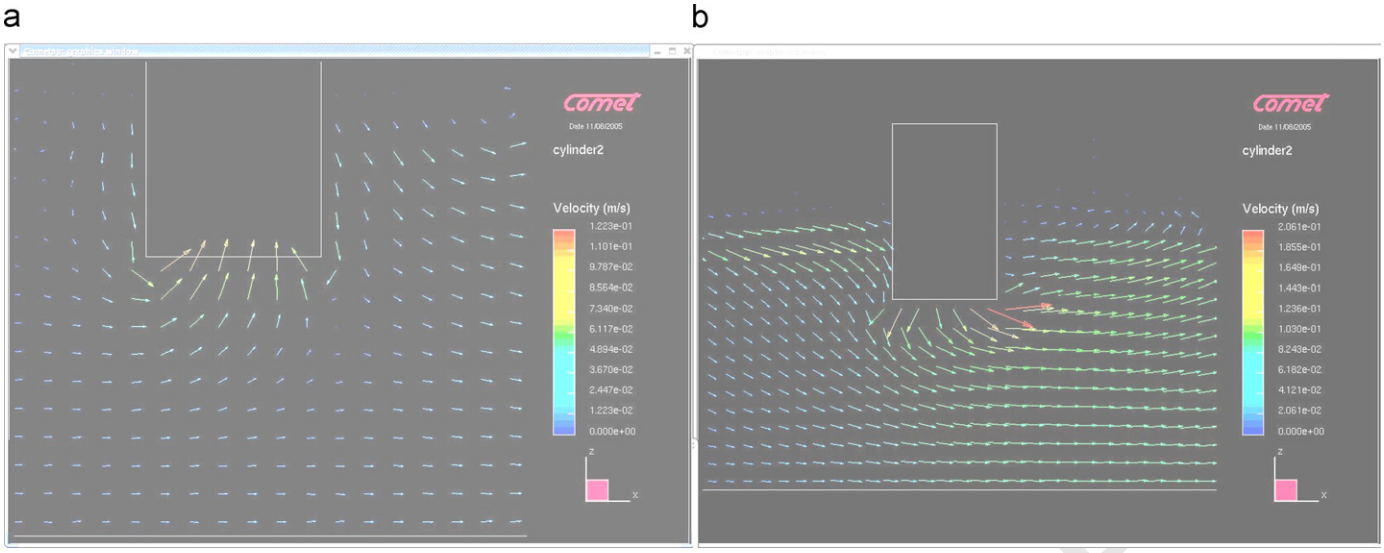

Fig. 7. Velocity vectors in heave oscillation: (a) buoy moving upwards; and (b) buoy moving downwards.

the simulation and therefore the power extraction is a function of the velocity. In this case, the PTO is represented as an ideal linear damper. The use of this "ideal condition" for energy extraction has enabled simplification of the process in order to demonstrate the technique. In future simulations non-linear damping can be incorporated. One potential advantage of the technique employed in this work is that, since the power extraction is computed in a FORTRAN user code that is linked to the CFD code, non-linear damping can easily be coded in the user files and these can be built into the iteration of the main code.

The power absorption damping coefficient b_1 depends on the type of PTO that is driven by the buoy. A simplified approach for incorporating the damping coefficient would be to express the torque or electrical output power of the generator in terms of the buoy or translator speed. The electrical power can be expressed in terms of the electromotive force and generator impedance; and the electromotive force is a function of the translator speed. For example, if a linear generator PTO is used, the coefficient would be a function of the translator position, load resistance, generator electrical parameters of the equivalent circuit and machine constants. This damping is generally non-linear and more complex, especially if the variation in frequency of the emf waveform is considered and power electronics is used for processing the output. The simplified approach is similar to investigating several generator loads for different wave conditions rather than calculating a damping coefficient.

Since the constant b_1 is directly proportional to the power captured, its value affects the output of the device. It has been established that for a buoy operating at resonance, a maximum amount of energy can be captured if the power take-off damping is equal to the hydrodynamic damping of the buoy [10]. This suggests the existence of an optimal value of damping for which power extraction can be maximized for each given wave condition.

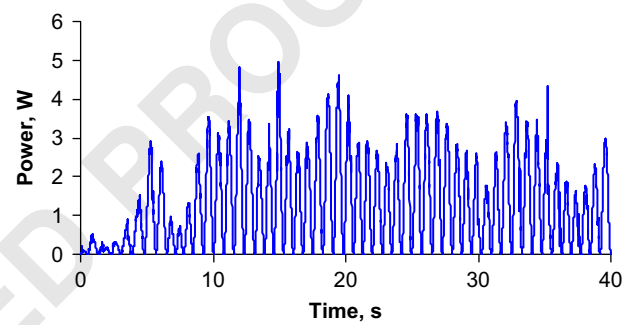

Fig. 8. Typical instantaneous power of OWEC.

The value of the PTO damping coefficient used for most of the simulations is 300 Ns/m. This was chosen based on the parameters of a new direct-drive device that was being designed at the time of the simulation. This device has been reported in [11]. Other damping coefficients investigated were 600 and 1000 Ns/m. The higher external damping coefficients enable the buoy to ride higher waves without being completely displaced out of the water.

3. Results

3.1. Response characteristics and power capture

The instantaneous power captured by the buoy depends on the PTO damping and the wave conditions. Fig. 8 shows the instantaneous power output from a wave condition of $H_s = 0.15$ and $T = 1.5$ s. This characteristic is typical for most of the wave conditions investigated. Also shown in Fig. 9 is instantaneous power with a wave period of $T = 2.5$ s and different wave heights of $H_{s1} = 0.6$ m and $H_{s2} = 0.15$ m. The peak power obtained from the wave conditions with H_{s1} is 12 times more than that of H_{s2}. The wave power is thus dependent non-linearly on the wave height. Estimations based on linear theory often give this

UNCORRECTED PROOF

Please cite this article as: Agamloh EB, et al. Application of fluid–structure interaction simulation of an ocean wave energy extraction device. Renew Energy (2007), doi:10.1016/j.renene.2007.04.010

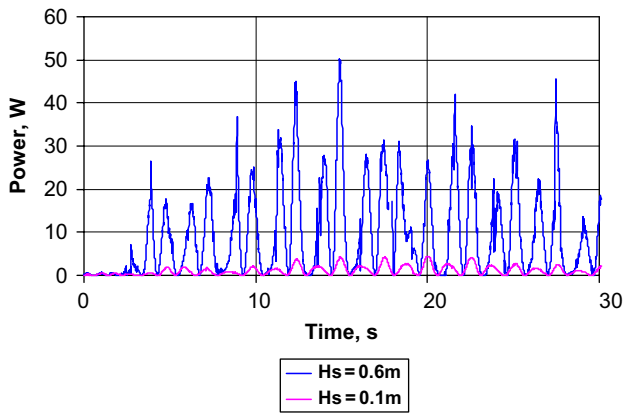

Fig. 9. Instantaneous power of OWEC in different waves.

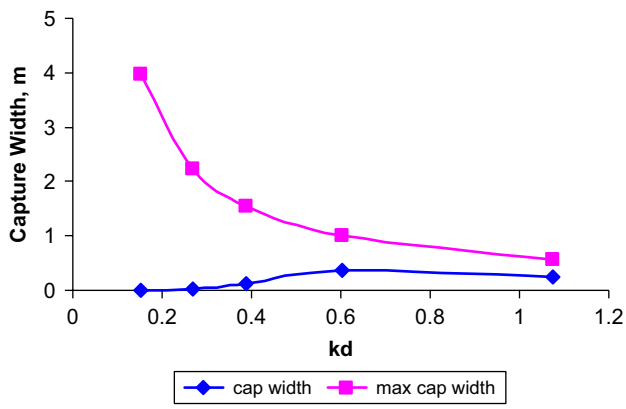

Fig. 10. Power absorption width from numerical model, $b_1 = 300\,\mathrm{Ns/m}$.

dependence as a quadratic dependence, which would have given 16 times more power.

3.2. Power capture width

The power capture or power absorption width of an OWEC is defined as

$$\lambda_{cap} = \frac{P_{cap}}{P_w}, \tag{16}$$

where P_{cap} is the power captured by the heaving buoy and P_w is the maximum power in the incident waves. The power absorption width of the single buoy system of the numerical model is given in Fig. 10 as a function of the kd, where k is the wave number and d is buoy diameter. As shown in Fig. 10, the capture width increases gradually as the resonance frequency for the device is approached. However, the capture width that was achieved is well below the theoretical maximum capture width of a point-absorber in heave defined by Budal and Falnes [12] as $\lambda/2\pi$, where λ is the wavelength. It can be seen that neither the generator damping nor the buoy geometry are optimal. With optimized buoy geometry, for example, a cylindrical buoy with a semi-sphere or conical base it would be possible to increase the power absorption width as reported in [13].

Table 1
Typical conversion efficiency

T (s)	H_s (m)	P (W)	P_{in} (W)	Conversion efficiency (%)
1.5	0.15	5	20	24.7
2	0.15	10	27	37.0
2.5	0.15	4.5	34	13.3
2.5	0.6	50	540	9.3
3	0.15	1.4	41	3.5
4	0.15	0.6	54	1.1

Also, control strategies are available that enable the power absorption to be increased [14].

The conversion efficiency of the energy extraction device is shown in the Table 1. The maximum conversion efficiency achieved was 37%. The output power was calculated as per Eq. (8) and the input power was calculated as $P_{in} = H_s^2 T \cdot d$ (kW), where d is the buoy diameter. The conversion efficiency depends on factors such as the wave conditions, buoy geometry and whether the buoy is controlled or not. A device that is oscillating with its natural frequency equal to the frequency of the incident waves (resonance) can achieve a conversion efficiency as high as the limit given in Fig. 10 at the resonance frequency but significantly less conversion efficiencies at other frequencies. If the device is controlled, then it has been shown that it can achieve considerably higher conversion efficiencies at various frequencies [14].

3.3. Application to existing energy extraction technologies

The leading generic technologies of ocean energy extraction are the oscillating water column and the point absorber. The oscillating water column converts the pneumatic energy in an air chamber into mechanical energy using the Well's turbine. This energy extraction technology has been extensively published in literature by researchers of Queen's University of Belfast.

The technique proposed here is applicable to floating bodies that directly interact with the ocean waves, such as buoy point absorbers in both spar and discus configurations. Preferably, the grid that is generated would apply to buoys that have a direct reaction force from the sea bed, as represented by rigid mooring. These buoys would normally be driving generator PTO mechanisms known as direct-drive [15,16]. In the present configuration, since the energy extraction is represented as a linear damper, other types of PTO mechanisms including hydraulic systems can also be applied to this technique. All that is required is the development of the solution domain representative of the buoy that is employed for the particular PTO mechanism.

The rigidly moored buoys are usually suitable for shallow water mounting, and in deep water slack-moored buoys are suitable. The configuration of buoy systems as slack-moored devices is often done with the help of a submerged drag plate. The relative motion between the plate and the buoy activates the PTO mechanism to extract

UNCORRECTED PROOF

Please cite this article as: Agamloh EB, et al. Application of fluid–structure interaction simulation of an ocean wave energy extraction device. Renew Energy (2007), doi:10.1016/j.renene.2007.04.010

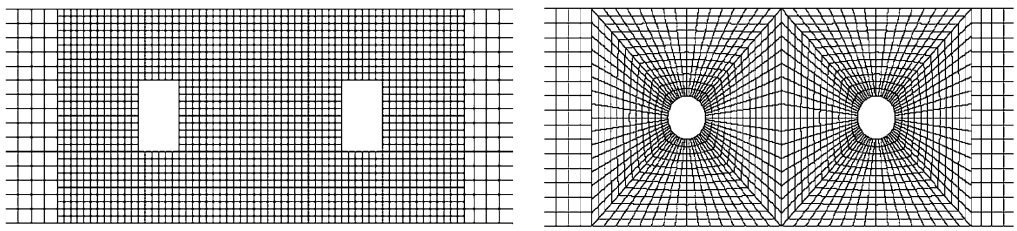

Fig. 11. Mesh around a double buoy system.

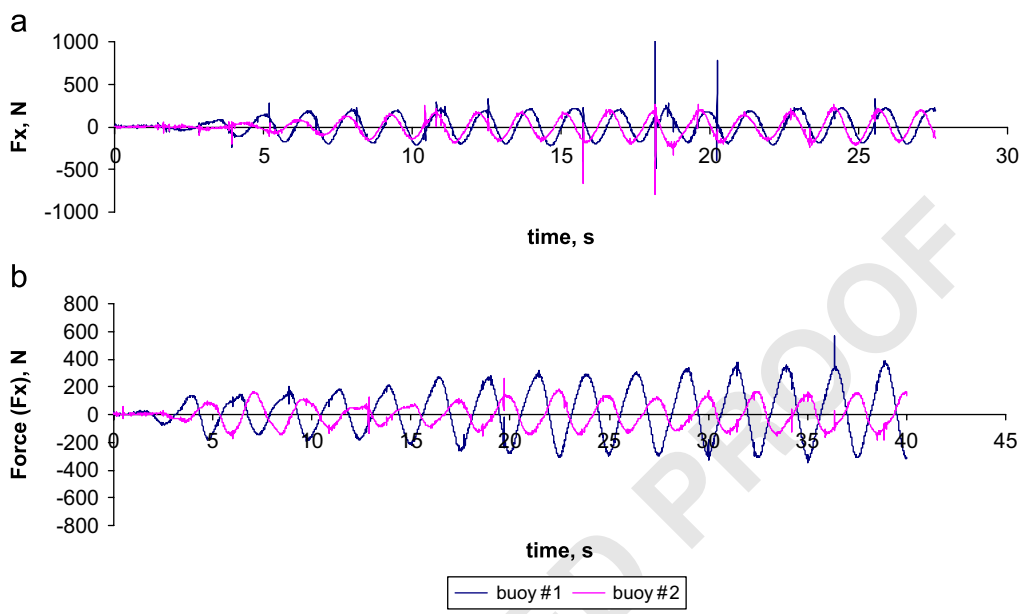

Fig. 12. In-line wave force on buoy array.

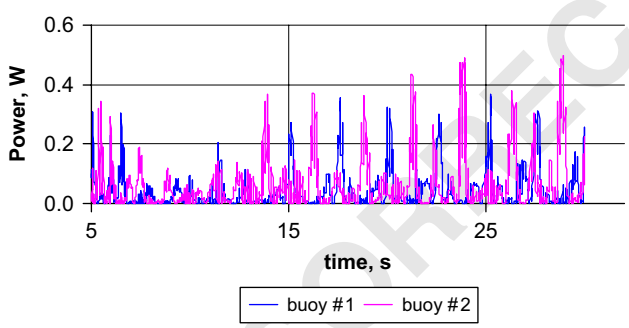

Fig. 13. Instantaneous power of buoy array ($T = 2.5$ s, $H_s = 0.2$ m).

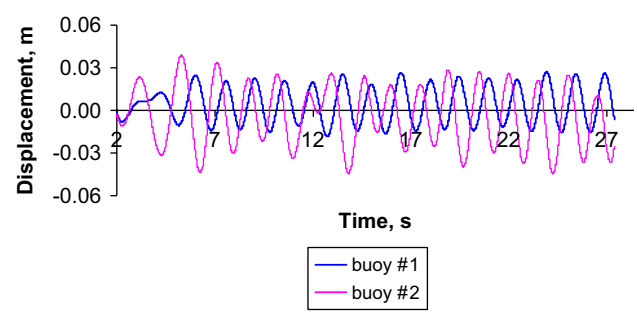

Fig. 14. Heave displacement of double buoy array $H_s = 0.15$ m, $T = 1.5$ s.

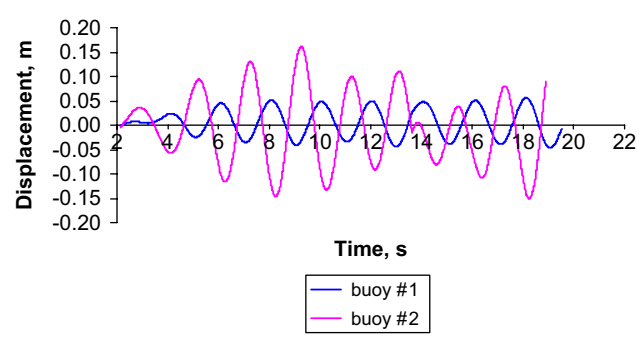

Fig. 15. Heave displacement of double buoy array $H_s = 0.15$ m, $T = 2$ s.

energy. When a drag plate is used, the buoy and the drag plate constitute different bodies and would have to be modeled as such. Depending on its location the interaction between plate and buoy could be significant. Due to these possible interactions the FSI model would be different and the current technique cannot be applied to a slack-moored system unless the significant changes are made in the model.

Experimental data on ocean energy extraction devices of the configuration and dimensions reported here are sparse. A device with similar dimensions of the geometry used in this simulation has been tested in irregular waves and

UNCORRECTED PROOF

Please cite this article as: Agamloh EB, et al. Application of fluid–structure interaction simulation of an ocean wave energy extraction device. Renew Energy (2007), doi:10.1016/j.renene.2007.04.010

reported in [11]. Further testing and research is on-going at Oregon State University that would provide additional data for future publications.

3.4. Double buoy array of OWECs

This section investigates the performance of an array of two buoys, heaving under the excitation of waves. The objective here is to investigate the effects of interactions between the devices and to determine how their performance compares to their operation as isolated OWECs.

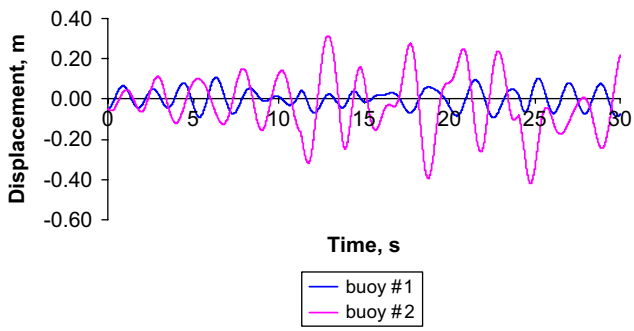

Fig. 16. Heave displacement of double buoy array $H_s = 0.15\,\mathrm{m}$, $T = 2.5\,\mathrm{s}$.

It has been shown through theoretical calculations, based on linear wave theory, that there is indeed interference between two or more point absorbers heaving in close proximity [17–19]. In general, the hydrodynamic interaction between neighboring bodies depends on their spacing, and can be constructive under certain wave conditions and destructive under others.

The system investigated comprises two identical buoy OWECs heaving in response to incident waves in a NWT. The dimension of the NWT is $15\,\mathrm{m} \times 3\,\mathrm{m} \times 3\,\mathrm{m}$ and the buoys are each of diameter 0.6 m and draft of 0.5 m. The buoys are initially spaced at a physical distance of 3 m and as the wavelength is changed the relative spacing to wavelength also changes. A typical grid surrounding the two buoys is shown in Fig. 11.

The effects of the separation between the two buoys can be observed in the in-line wave forces on the two buoys. Fig. 12 shows these forces on the two cylindrical buoys as a result of wave excitation. As the distance between the two buoys is increased, the forces on the second buoy lag by a

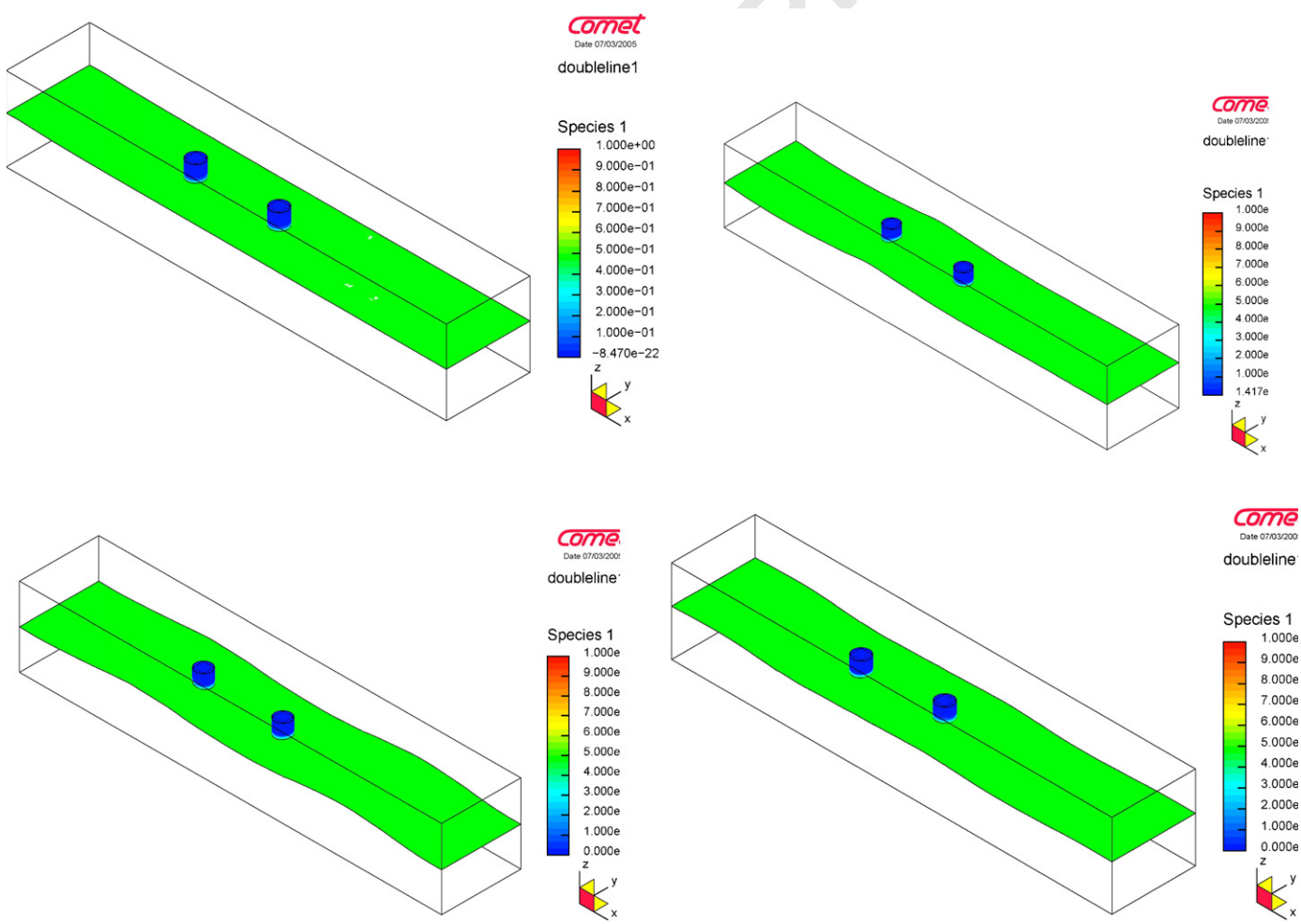

Fig. 17. Free surface capturing of double buoy array.

Please cite this article as: Agamloh EB, et al. Application of fluid–structure interaction simulation of an ocean wave energy extraction device. Renew Energy (2007), doi:10.1016/j.renene.2007.04.010

wider margin. Also, the amplitude changes in Fig. 12b are due to interference effects of the two buoys.

The location of the two buoys apart also helps smooth out the instantaneous power output of the plant. As shown in Fig. 13, the shift in phase of the two buoy systems enables the troughs in instantaneous power of one device to be filled by peaks of the other device. This has little effect on the intermittency of the output but would help to alleviate the power output processing requirements, especially where a large number of buoys are involved.

The heave displacements in Figs. 14–16 show some interaction between the two buoys. In the cases presented, the amplitude of motion of the second buoy is higher than the first buoy. The first buoy has experienced a reduction in amplitude compared to the isolated case, while the second has experienced an increase in amplitude over the isolated case. The case in Fig. 16 shows severe interactions of the displacements compared to Figs. 14 and 15. Though the initial investigations show some interaction between the two devices, more simulations are needed and are being pursued in order to fully quantify the effects more comprehensively.

The free surface capture of the array is shown in Fig. 17, with the two buoys initially neutrally buoyant.

4. Conclusion

A numerical method was presented in this paper to demonstrate the use of FSI to simulate an OWEC device. The CFD code employed (COMET) is a finite volume code that has been widely used and validated in previous published works and provides efficient algorithms and mathematical models for the simulation of continuum mechanics problems.

The buoy investigated in this work has a simple cylindrical shape, but the structure of existing device prototypes is more complex than smooth cylinders. However, the procedures developed in this work can be used in applying commercially available fluid solvers to simulate FSI and determine the power output of an OWEC device. For more complex buoy shapes, further work would be needed to use external mesh generation algorithms and programs to create more complex grids that replicate the shape of real buoys and then import these grids into commercial codes to solve.

This work was expanded to include multiple buoy systems to investigate optimum buoy spacing for wave park arrays, similar to wind farms. However, this requires significant computational resources and more simulation runs will be pursued in order to fully quantify the interference effects more comprehensively.

Acknowledgment

While this paper was being reviewed for publication, Dr. Alan K. Wallace passed away after a brief illness on June 7, 2006. The authors dedicate this paper to the memory of their friend, colleague and mentor.

References

[1] Azcueta R, Hadzic I, Muzaferija S, Peric M. Computation of flows with free surface. First MARNET CFD workshop, Barcelona, 1999.
[2] Azcueta R, RANSE simulations for sailing yachts including dynamic sinkage and trim and unsteady motions in waves. High performance yatch design conference, Auckland, 2002.
[3] Sakar T, Vassalos D. A RANS based technique for simulation of the flow near a rolling cylinder at the free surface. J Marine Sci Technol 2000;5:66–77.
[4] Tanizawa K, Naito S. A study on parametric roll motions by fully non-linear numerical wave tank. 7th ISOPE conference, May 1997.
[5] Dean RG, Darymple RA. Water wave mechanics for engineers and scientists. Singapore: World Scientific; 1991.
[6] Yueng RW, Ananthakrishnan P. Oscillation of a floating body in a viscous fluid. J Eng Math 1992;26:211–30.
[7] CCM GmbH. Comet v.2 user manual. Germany: 2001.
[8] Azcueta R, Computation of turbulent free-surface flows around ships and floating bodies. PhD thesis, Technischen Universitat Hamburg, Harburg, 2001.
[9] Muzaferija S, Peric M, Computation of free surface flows using interface-tracking and interface-capturing methods, In: Mahrenholtz O, Markiewicz M, editors. Nonlinear water wave interaction. WIT Press; 1999. p. 59–100.
[10] Mei CC. Power extraction from water waves. J Ship Res 1976;20(2):63–6.
[11] Agamloh EB, Wallace AK, von Jouanne A. A novel direct-drive ocean energy extraction concept with contact-less force transmission system. Renewable Energy, to appear.
[12] Budal K, Falnes J. Interacting point absorbers with controlled motion. In: Count BM, editor. Power from sea waves. New York: Academic Press; 1980. p. 381–99.
[13] Vantore M, Banasaik R, Verhoeven R. Modeling of hydraulic performance and wave energy extraction by a point absorber. Appl Ocean Res 2004;26:61–72.
[14] Babarit A, Duclos G, Clement AH. Comparison of latching control strategies for heaving wave energy device in random sea. Appl Ocean Res 2004;26:227–38.
[15] Mueller MA. Electrical generators for direct drive wave energy converters. Proc IEE Gen Trans Distr 2002;149(4).
[16] Rhinefrank K, Agamloh EB, von Jouanne A, Wallace AK, Prudell J, Kimble K, et al. A novel ocean energy permanent magnet linear generator buoy. Renewable Energy 2006;31(9):1279–98.
[17] Budal K. Theory for absorption of wave power by a system of interacting bodies. J Ship Res 1977;21:248–53.
[18] Evans DV. Some theoretical aspects of three dimensional wave energy absorbers. Proceedings of the first symposium on wave energy utilization, Chalmers University of Technology, Gothenburg, Sweden, 1979. p. 77–106.
[19] McIver P. Some hydrodynamic aspects of arrays of wave-energy devices. Appl Ocean Res 1994;16:61–9.

UNCORRECTED PROOF

Please cite this article as: Agamloh EB, et al. Application of fluid–structure interaction simulation of an ocean wave energy extraction device. Renew Energy (2007), doi:10.1016/j.renene.2007.04.010